Linear stability of buoyant convective flow in a vertical channel with internal heat sources and a transverse magnetic field

Hudoba, A. and Molokov, S.

Author post-print (accepted) deposited by Coventry University's Repository

Original citation & hyperlink:
Hudoba, A. and Molokov, S. (2016) Linear stability of buoyant convective flow in a vertical channel with internal heat sources and a transverse magnetic field. Physics of Fluids, volume 28 : 114103
http://dx.doi.org/10.1063/1.4965448

DOI 10.1063/1.4965448
ISSN 1070-6631
ESSN 1089-7666

Publisher: AIP Publishing

This article may be downloaded for personal use only. Any other use requires prior permission of the author and AIP Publishing.

The following article appeared in Hudoba, A. and Molokov, S. (2016) Linear stability of buoyant convective flow in a vertical channel with internal heat sources and a transverse magnetic field. Physics of Fluids, volume 28 : 114103 and may be found at http://dx.doi.org/10.1063/1.4965448

Copyright © and Moral Rights are retained by the author(s) and/ or other copyright owners. A copy can be downloaded for personal non-commercial research or study, without prior permission or charge. This item cannot be reproduced or quoted extensively from without first obtaining permission in writing from the copyright holder(s). The content must not be changed in any way or sold commercially in any format or medium without the formal permission of the copyright holders.

This document is the author's post-print version, incorporating any revisions agreed during the peer-review process. Some differences between the published version and this version may remain and you are advised to consult the published version if you wish to cite from it.

Linear stability of buoyant convective flow in a vertical channel with internal heat sources and a transverse magnetic field

A. Hudoba[1, a)] and S. Molokov[1]
School of Computing, Electronics and Mathematics, Coventry University, Priory Street, Coventry CV1 5FB, United Kingdom

(Dated: 5 October 2016)

Linear stability of buoyant convective flow of an electrically conducting fluid in a vertical channel owing to internal heat sources has been studied. The flow takes place in a transverse, horizontal magnetic field. The results show that up to four different local minima may be present in the neural stability curve. Up to two of these modes may be the most unstable depending, critically, on the value of the Hartmann number. Over a wide range of moderate to high Hartmann numbers thermal waves dominate the instability. As the Hartmann number increases, however, this mode is strongly damped. Then the so-called Hartmann mode takes over, which involves the characteristic Hartmann layers at the walls appearing due to modification of the basic velocity profile by the magnetic field. Overall, for liquid metals at high magnetic fields the basic flow is very stable. Variation of the Prandtl number in a wide range has also been performed as, depending on the type of an electrically conducting fluid (liquid metal or various kind of electrolytes), the Prandtl number varies over several orders of magnitude. As may be expected, the increase of the Prandtl number lowers the instability threshold for the thermal waves.

I. INTRODUCTION

Over many years several concepts of liquid metal blankets for thermonuclear reactors have been developed[1]. The main aims of these devices is to cool the reactor first wall, to breed tritium, or both[2–4]. The flow in the blankets occurs in the presence of a high magnetic field of between 5 and 12 Tesla, so that the flowing liquid metal experiences the action of strong, braking, electromagnetic forces. In addition, the velocity profiles are highly affected forming various type of thin boundary layers at the duct walls. The geometry of the ducts is usually very complex, involving expansions, bends, manifolds, etc. The main elements of the blankets, however, are horizontal or vertical rectangular ducts, depending on the concept. Here we will focus on vertical ducts.

An important factor to consider for all the blanket designs is neutron irradiation resulting in internal volumetric heating of the flow. The stability of mixed convection in ducts under fusion reactor blanket conditions has been studied in the presence of a transverse magnetic field[5–7] in the quasi-two-dimensional approximation, which applies only for thermally and electrically insulating walls transverse to the magnetic field. The background temperature field is supposed to vary across, not along the field. When these conditions are not fulfilled, the analysis does not apply. To get a clear picture of the effect of internal heating on the magnetohydrodynamic (MHD) flow all possible types and combinations of the boundary conditions are of interest. In this study we will focus on the flow in a vertical channel in a transverse field, assuming that the aspect ratio of the duct is sufficiently high, so that the lateral walls are removed to infinity. The fluid is heated by the internal heat sources and cooled at the walls (Figure 1).

The non-magnetic problem of a convective flow in a vertical channel with uniformly distributed internal heat sources and with walls maintained at constant and equal temperatures has been discussed in detail in Refs. 8, 9 and 10. The results have been obtained first under conditions where the effects of thermal perturbations are negligible[8]. Stability of flow has been studied in a hydrodynamic formulation by the solution of the Orr-Sommerfeld eigenvalue problem with a given velocity profile. In the further works[9,10] thermal perturbations have been taken into account. The main conclusion was that for low values of the Prandtl number the instability develops at the boundaries between the counter flows. As the thermal effects increase, the hydrodynamic instability turns into the instability of the type of thermal waves. This transition occurs continuously owing to a peculiar feature of the marginal stability curve. For low values of the Prandtl number, a single minimum exists. With its increase, the curve forms a second local minimum, then a cusp, and then a loop, corresponding to the mode of dynamic origin.

Stability of a convective flow in the same geometry has been also studied in the presence of a transverse magnetic field[11] for low values of the Hartmann number (up to 10). As expected, these results show the stabilizing effect of a transverse magnetic field.

[a)] ac0640@coventry.ac.uk

The goal of this work is to provide a complete linear stability analysis of the flow induced by uniformly distributed heat sources and confined between two parallel vertical plates, and to understand the instability mechanisms when the external magnetic field increases from zero to high values. The problem is considered assuming a fully developed flow, realized in the middle portion of a sufficiently long vertical channel, where the end effects from a top and bottom lids of a cavity are negligible. This allows very accurate analysis of the instabilities by pseudospectral methods. The presence of the lids, however, is kept in mind, so that the flow rate in the channel is equal to zero.

II. FORMULATION

Consider a time-dependent, convective flow of a viscous, electrically conducting fluid subject to a uniform externally applied magnetic field $\mathbf{B}_0 = B_0\mathbf{e}_x$ in the presence of gravity $\mathbf{g} = -g\mathbf{e}_z$, where g is the gravitational acceleration. We choose Cartesian coordinate system (x, y, z) with the origin located in the mid-plane of the channel, where the rigid boundaries are situated at finite values of the $x-$ coordinate and all the body forces act in the $(x - z)$ plane (Figure 1). It is assumed that the horizontal extension of the plates is large so that the lateral walls do not affect the flow.

The two parallel vertical rigid boundaries are maintained at constant and equal temperature, T_w. Convective motion is induced by internal heat sources of uniform volume density Q distributed through the channel. If the vertical extension of the channel is sufficiently large and end effects at distant walls in the $z-$ direction can be omitted, the parabola-type temperature profile is established[8]. This leads to a symmetric plane-parallel steady flow consisting of three convective streams: the central upstream and two downstreams at the walls.

Material parameters of the fluid are defined by the density ρ, kinematic viscosity ν, thermal diffusivity κ, thermal expansion coefficient β, electric conductivity σ and specific heat at constant pressure c_p.

It is convenient to present the governing equations in a dimensionless form by scaling the length by the distance between walls d, time t by d^2/ν, velocity $\mathbf{v}$ by ν/d, pressure p by $\rho\nu^2/d^2$, electric potential ϕ by $B_0\nu$, temperature $T - T_w$ by a typical temperature difference $\Delta T = Qd^2/\nu\rho c_p$ and magnetic field by B_0. The following nondimensional numbers are introduced as control parameters:

$$Gr = \frac{g\beta\Delta T d^3}{\nu^2}\ , \quad Ha = B_0 d\sqrt{\frac{\sigma}{\rho\nu}}\ , \quad Pr = \frac{\nu}{\kappa}\ . \tag{1}$$

Here the strength of buoyancy forces is characterized by the Grashof number, Gr, the ratio of the electromagnetic to viscous forces is defined by the square of the Hartmann number, Ha, while the Prandtl number, Pr, depending solely on the fluid properties, measures the ratio of the kinematic viscosity to the thermal diffusivity.

The problem is considered in the so-called inductionless approximation for low values of the magnetic Prandtl number, $Pr_m = \mu_0\sigma\nu << 1$. Here μ_0 stands for the magnetic permeability of vacuum. According to this approximation, an induced magnetic field due to fluid flow is assumed to be negligible[12].

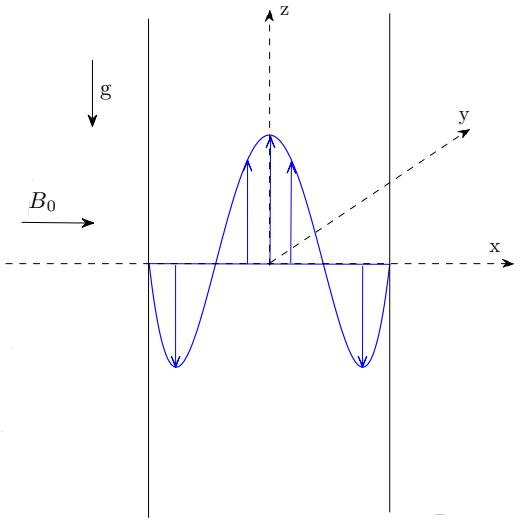

FIG. 1. Schematic diagram of the vertical fluid layer with side walls of equal temperatures and uniform internal heating. The total flow rate is equal to zero.

The density-temperature relationship is assumed to follow the usual Boussinesq approximation for incompressible fluids[13], with $\rho = \rho_0(1 - \beta(T - T_w))$, where ρ_0 is the density of the fluid at a wall temperature. The resulting set of nondimensional equations governing the motion of the fluid is:

$$\frac{\partial \mathbf{v}}{\partial t} + (\mathbf{v} \cdot \nabla)\mathbf{v} = -\nabla p + \nabla^2 \mathbf{v} + Ha^2(-\nabla\phi + \mathbf{v} \times \mathbf{e}_x) \times \mathbf{e}_x + GrT\hat{\mathbf{e}}_z \ , \tag{2}$$

$$\frac{\partial T}{\partial t} + (\mathbf{v} \cdot \nabla)T = \frac{1}{Pr}\nabla^2 T + 1 \ , \tag{3}$$

$$\nabla \cdot \mathbf{v} = 0 \ , \tag{4}$$

$$\nabla^2 \phi = \mathbf{e}_x \cdot (\nabla \times \mathbf{v}). \tag{5}$$

The boundary conditions at $x = \pm\frac{1}{2}$ are:

$$\mathbf{v} = 0 \ , \quad T = 0 \ . \tag{6}$$

Although in general the electric conductivity of the walls may vary, the electric boundary conditions never enter the analysis and have no effect on the stability of the flow for the problem considered. We discuss this in more detail in section IV.

III. BASIC FLOW

We will be interested here in the linear stability of a flow resulting from the buoyant convection due to internal heating. In order to perform the stability analysis of the system described above, first the equilibrium state needs to be defined.

The problem has a steady basic flow, with the single-component velocity profile $\mathbf{w}_0 = [0, 0, w_0(x)]$ and the basic temperature profile $T_0(x)$ (Figure 2), governed by the following set of equations:

$$w_0''' - Ha^2 w_0' + GrT_0' = 0 \ , \tag{7}$$

$$T_0'' + Pr = 0 \ , \tag{8}$$

as follows from Eqs. (2)−(5). Here the prime symbol ($'$) denotes the derivative with respect to x.

As we consider here the case of a closed channel at high values of $|z|$, the total flux of flow across a horizontal plane vanishes:

$$\int_{-1/2}^{1/2} w_0 \, \mathrm{d}x = 0 \ . \tag{9}$$

The analytical expressions for the basic velocity $w_0(x)$ and temperature $T_0(x)$ profiles[11], being even functions with respect to the channel axis, are:

$$w_0 = \frac{PrGr}{2Ha^2}\left\{-x^2 + \frac{2Ha\cosh(Hax) - 6\sinh(0.5Ha) + Ha\cosh(0.5Ha)}{12Ha\cosh(0.5Ha) - 24\sinh(0.5Ha)}\right\} \ , \tag{10}$$

$$T_0 = \frac{1}{2}Pr\left\{-x^2 + \frac{1}{4}\right\} \ . \tag{11}$$

The temperature profile does not depend on the Hartmann number, and thus is identical with the case of natural convection in the absence of the magnetic field.

For the unidirectional stationary channel flow, which is independent of the $y-$ and $z-$coordinates, there is only one non-zero component of current $j_{y,0}$, and the electric field $E_0 = constant$. From Ohm's law for the fluid follows:

$$j_{y,0} = E_0 - w_0 \ . \tag{12}$$

For the walls,

$$j^{\pm}_{y,0} = \sigma^{\pm} E_0 \ , \tag{13}$$

where $j^{\pm}_{y,0}$, $\sigma^{\pm}$ are the dimensionless electric current and electrical conductivity for walls at $x = +\frac{1}{2}$ and $x = -\frac{1}{2}$, respectively.

Integrating Eq. (12) across the channel and taking into account Eq. (9) gives:

$$I_0 = E_0 \ . \tag{14}$$

The total current flowing in the fluid and the walls must be zero. Thus,

$$I_0 + \int_{-\frac{1}{2}-h^-}^{-\frac{1}{2}} j^{-}_{y,0} \mathrm{d}x + \int_{\frac{1}{2}}^{\frac{1}{2}+h^+} j^{+}_{y,0} \mathrm{d}x = 0 \ , \tag{15}$$

where $h^{\pm}$ are dimensionless thicknesses of the walls at $x = +\frac{1}{2}$ and $x = -\frac{1}{2}$, respectively. Substituting Eqs. (14) and (13) into Eq. (15) yields:

$$E_0 \left(1 + c^+ + c^-\right) = 0 \ , \tag{16}$$

where $c^{\pm} = \sigma^{\pm} h^{\pm}$ are the wall conductance ratios of the walls at $x = +\frac{1}{2}$ and $x = -\frac{1}{2}$, respectively. The above equation implies that the electric field vanishes, so that $\nabla \phi_0 = -E_0 \mathbf{e}_y = 0$, which implies in turn that ϕ_0 is a constant. Thus it can be set to zero as a reference potential:

$$\phi_0 = 0 \ , \tag{17}$$

throughout the domain for any wall conductance ratios of the walls. The reason for this is that the electric currents do not flow in the walls due to $E_0 = 0$, which is a direct consequence of the flow rate through the channel being zero.

The upward fluid motion due to internal heat sources must be compensated for a closed cavity. This is done by the induced pressure gradient:

$$\frac{\mathrm{d}p_0}{\mathrm{d}z} = PrGr \left\{ \frac{1}{8} - \frac{1}{Ha^2} + \frac{6\sinh(0.5Ha) - Ha\cosh(0.5Ha)}{24Ha\cosh(0.5Ha) - 48\sinh(0.5Ha)} \right\} \ . \tag{18}$$

Further examination of the basic flow shows that the inflection points in the velocity distribution, where $\mathrm{d}^2 w_0 / \mathrm{d}x^2 = 0$, appear at the values of x_i given by:

$$f_i = \cosh(Hax_i) = \frac{C_1}{Ha^3} \ , \tag{19}$$

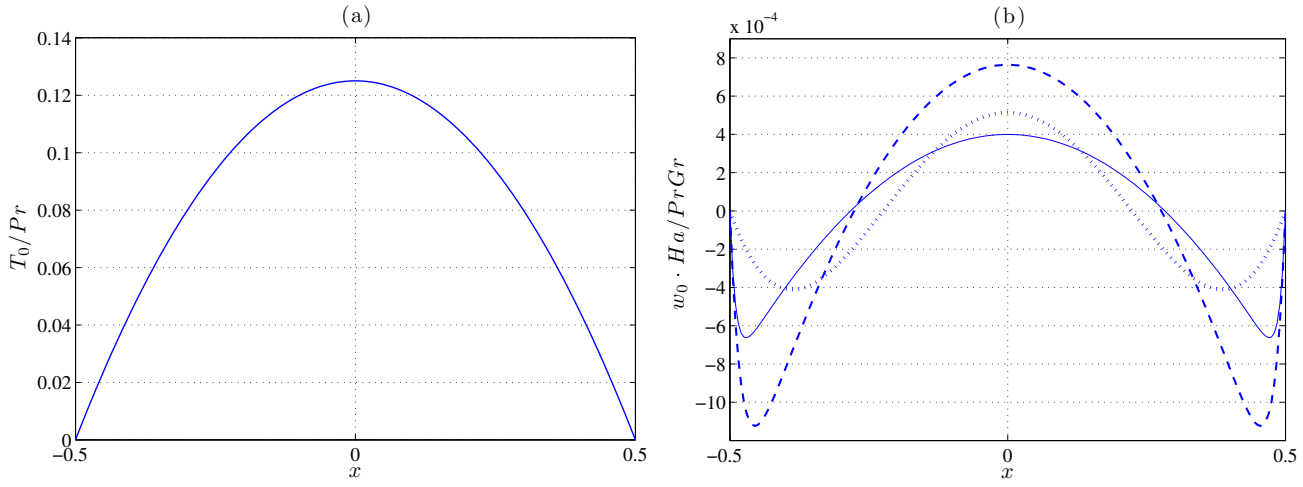

FIG. 2. Basic temperature profile (a) and basic velocity profile for $Pr = 0.015$ (b) for $Ha = 1$ (dotted line), $Ha = 50$ (broken line) and $Ha = 100$ (solid line). The basic temperature is scaled here by Pr, the basic velocity is scaled by $PrGr/Ha$.

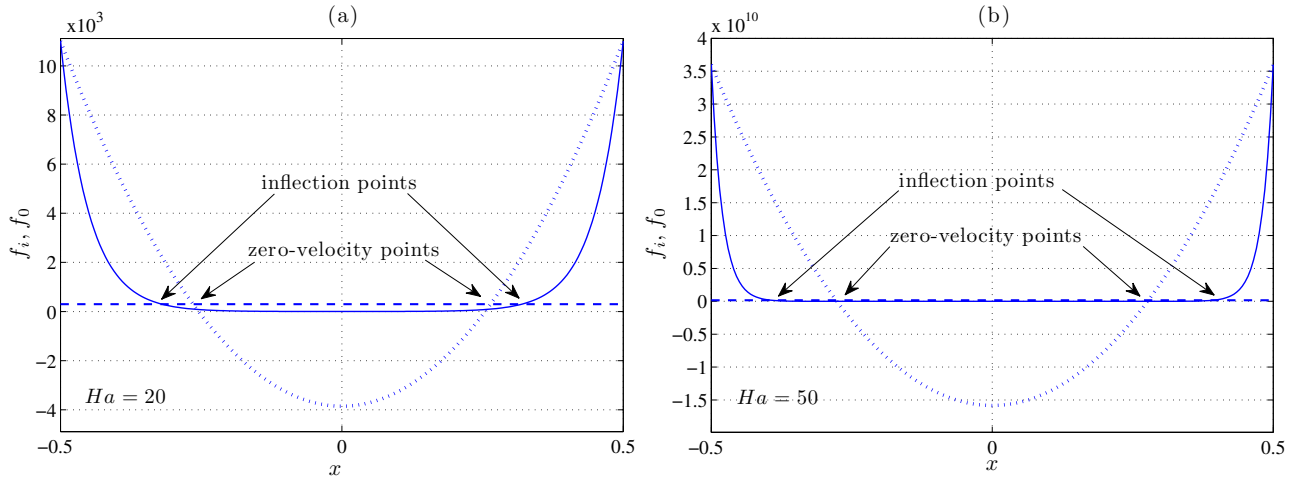

FIG. 3. Inflection and zero-velocity points of the steady-state velocity profile for $Ha = 20$ (a) and $Ha = 50$ (b). The location of inflection points along the $x-$ direction is given by the intersection of $\cosh(Hax)$ (solid lines) with a constant function (broken lines). The points of zero velocity are given by the intersection of $\cosh(Hax)$ with a quadratic function of x (dotted lines).

which do not correspond to the points of zero velocity between convective counterflows, x_0, given by:

$$f_0 = \cosh(Hax_0) = \frac{C_1 x_0^2 - C_2}{2Ha} \ . \tag{20}$$

Here $C_1 = 12\{Ha\cosh(0.5Ha) - 2\sinh(0.5Ha)\}$ and $C_2 = Ha\cosh(0.5Ha) - 6\sinh(0.5Ha)$.

With the increasing values Ha, the inflection points in the velocity profile drift further apart from the points of zero velocity towards the channel walls, as shown in Figure 3a for $Ha = 20$ and Figure 3b for $Ha = 50$. The leading terms of the asymptotics for the position of the inflection and zero-flow points are:

$$x_i \cong \pm\left\{\frac{1}{2} - \frac{2\ln(Ha)}{Ha}\right\} \ , \tag{21}$$

$$x_0 \cong \pm\frac{1}{\sqrt{12}} \ . \tag{22}$$

From the expression (21) follows that the lines of inflection move right into the Hartmann layers.

At high values of the Hartmann number, $Ha >> 1$, the full basic velocity profile (10) can be replaced by the following asymptotic profile:

$$w_0 = \frac{PrGr}{2Ha^2}\left\{-x^2 + \frac{Ha-6}{12Ha-24} + \frac{Ha}{6Ha-12}\left(e^{Ha(x-0.5)} + e^{-Ha(x+0.5)}\right)\right\} \ , \tag{23}$$

where the first two terms in brackets represent the core velocity, while the third term corresponds to the Hartmann-layer corrections.

In this study, three values of the Prandtl number, $Pr = 0.015$, 7.01, 38.055, were chosen for sample calculations, corresponding to the cases of liquid metals, water-based electrolytes and Flibe[14], respectively.

The reason for choosing such a wide range of Pr is the following. First of all, for liquid metals, Pr is very small, i.e. they are good thermal conductors. Liquid metals are most relevant materials for blankets. Secondly, water-based electrolytes have been proposed for visualization of magnetohydrodynamic (MHD) convection[15] as the liquid metals are opaque making the direct visualization of flow impossible. Finally, Flibe[14] has been proposed as a replacement of liquid metal for blanket design. As all the electrolytes it has low electrical conductivity but high Prandtl number. As we will see below, the instability mechanisms may be completely different depending on the type of the fluid.

The magnetic field in a fusion blanket can reach very high values of $10 - 12$ Tesla. For a channel of width $d = 5$ cm, in the parameter ranges considered, corresponding values of the Hartmann number are $Ha \sim 10^4$ for eutectic lead lithium alloy, and $Ha \sim 10^2$ for Flibe. In experiments performed under magnetic fields up to 5 Tesla, the corresponding Hartmann numbers are $Ha \sim 10^3$ for liquid metals, and $Ha \sim 10^1 - 10^2$ for water-based electrolytes.

The dimensionless parameters and scales introduced in Eq. (1) allow to conclude the insignificance of the Joule heating effect for all three kinds of working fluids[16–18] in the parameter range considered. In a channel of width $d = 5$ cm, the ratio of the Joule heating (j^2/σ) to the internal heating source Q, is of order $10^{-7} - 10^{-8} \cdot Ha^2/Gr$. Thus the effects of the Joule heating may be neglected. From Eq. (12) with $E_0 = 0$ follows that the electric currents in the Hartmann layers have the same scaling as those in the core of the flow, so the same estimate for these layers is valid. This contrasts with flows with non-zero flow rate where such currents are higher by a factor of Ha or by $1/c^{\pm}$, whatever is higher. For estimates of the importance of Joule heating in pressure-driven channel flows for blanket-relevant conditions see Ref. 19. More generally, Joule heating is important mainly for flows driven by sufficiently strong, externally imposed electric current crossed by the magnetic field.

IV. DISTURBANCE EQUATIONS AND ENERGY ANALYSIS

The stability is investigated here by the linear analysis. Assuming that disturbances to the flow are fully three-dimensional, the flow can be decomposed into the basic flow and the fluctuating component $F = F_0 + f(x, y, z, t)$. Additionally the perturbations can be expressed with Fourier expansions in the $y-$ and $z-$ directions $f(x, y, z, t) = \hat{f}(x) \exp\{iyk_y + izk_z + \lambda t\}$, where k_y and k_z are the wavenumbers in the $y-$ and $z-$ directions, respectively. Here $\lambda = \lambda_r + i\lambda_i$ is a complex eigenvalue of perturbations with real part λ_r representing their growth rate while $\lambda_i -$ their angular oscillation frequency.

Assuming that the introduced perturbation is infinitesimally small, the problem (2)$-$(5) is linearized at the vicinity of the steady state (10)$-$(11) and all the products of perturbations are neglected. Additionally, in order to reduce the number of variables, the vorticity vector is introduced $\omega = \nabla \times \mathbf{v}$. This leads to the following set of equations for the disturbed velocity, vorticity, temperature and the disturbed electric potential:

$$\{\mathbf{D}^4 - w_0 ik_z \mathbf{D}^2 + w_0'' ik_z - Ha^2 \frac{\mathrm{d}^2}{\mathrm{d}x^2}\}\hat{u} - Grik_z \frac{\mathrm{d}\hat{\theta}}{\mathrm{d}x} = \lambda \mathbf{D}^2 \hat{u} \ , \tag{24}$$

$$\{\frac{1}{Pr}\mathbf{D}^2 - w_0 ik_z\}\hat{\theta} - T_0' \hat{u} = \lambda \hat{\theta} \ . \tag{25}$$

$$\{\mathbf{D}^2 - w_0 ik_z\}\hat{\omega}_x - w_0' ik_y \hat{u} + Grik_y \hat{\theta} - Ha^2 \frac{\mathrm{d}^2 \hat{\phi}}{\mathrm{d}x^2} = \lambda \hat{\omega}_x \ , \tag{26}$$

$$\hat{\omega}_x = \mathbf{D}^2 \hat{\phi} \ , \tag{27}$$

Here the operator $\mathbf{D} = i\mathbf{k} + [\frac{\mathrm{d}}{\mathrm{d}x}, 0, 0]$ has been introduced.

As in the non-magnetic flow, the system of governing disturbance equations separates into two sets, and an independent set consisting of equations (24) and (25) can be solved separately. Equations (26) and (27) involving disturbed vorticity and electric potential can be omitted as the Squire modes are stable with or without the transverse magnetic field[20]. Further, for Eqs. (24) and (25) Squire's theorem is valid, which can be easily shown similarly to Ref. 20. Through a straightforward transformation, Eqs. (24)$-$(25) can be reduced to an equivalent set of two-dimensional equations. Substituting the polar wavenumber, $k = \sqrt{k_y^2 + k_z^2}$, and a reduced Grashof number, $Gr_{2d} = Grk_z/k$, the disturbed velocity (24) and temperature (25) equations can be written as:

$$\{\mathbf{D}^4 - \tilde{w}_0 ik\mathbf{D}^2 + \tilde{w}_0'' ik - Ha^2 \frac{\mathrm{d}^2}{\mathrm{d}x^2}\}\hat{u} - Gr_{2d} ik \frac{\mathrm{d}\hat{\theta}}{\mathrm{d}x} = \lambda \mathbf{D}^2 \hat{u} \ , \tag{28}$$

$$\{\frac{1}{Pr}\mathbf{D}^2 - \tilde{w}_0 ik\}\hat{\theta} - T_0' \hat{u} = \lambda \hat{\theta} \ . \tag{29}$$

Here $\tilde{w}_0$ is the basic velocity profile (10) for the reduced Grashof number, Gr_{2d}. Thus the problem with three-dimensional disturbances has been reduced to the two-dimensional one. Note that for convection in a horizontal layer[21,22] this is not the case. For flows in an aligned field this is not the case either[23].

The appropriate boundary conditions are imposed at the solid isothermal side walls, where the velocity and temperature perturbations vanish and hence:

$$\hat{u} = \frac{\mathrm{d}\hat{u}}{\mathrm{d}x} = \hat{\theta} = 0 \qquad \text{at} \quad x = \pm\frac{1}{2} \ . \tag{30}$$

Note that the electric potential does not enter the analysis and the electric conductivity of the side walls plays no role in this problem.

Equations (24)−(25), together with the boundary conditions (30) constitute a boundary value problem, which defines the spectrum of perturbations. The flow is stable for $\lambda_r < 0$, neutrally stable for $\lambda_r = 0$ or unstable when $\lambda_r > 0$. The stability criteria are determined here in terms of the critical Grashof number, Gr_{cr}, as a function of various parameters. Neutral stability results have been calculated for fixed values of Pr and Ha, and then the dependence of Gr_{cr} on these parameters is studied.

A. Energy Considerations

The perturbation energy analysis is performed for better understanding of the instability mechanisms. The equations for energy components can be derived from the governing equations: the fluctuating kinetic energy from the momentum equation (2) and the fluctuating thermal energy from the temperature equation (3). These equations are studied in order to establish different energy contributions corresponding to specific instabilities.

Following the approach in Ref. 21, the governing perturbation equations are multiplied by the corresponding complex conjugates (denoted here with an asterisk) and integrated along the $x-$ direction. The real parts of the resulting equations give the desired energy balances.

The rate of change of the fluctuation kinetic energy K:

$$\mathrm{Re}\left(\frac{\mathrm{d}K}{\mathrm{d}t}\right) = \mathrm{Re}\left(\lambda \int_x \hat{\mathbf{v}} \cdot \hat{\mathbf{v}}^* \mathrm{d}x\right) = K_d + K_f + K_b + K_m \ , \tag{31}$$

where $K = \int_x \hat{\mathbf{v}} \cdot \hat{\mathbf{v}}^* \mathrm{d}x$, with the viscous dissipation of fluctuating kinetic energy K_d :

$$K_d = \mathrm{Re}\left(\int_x \mathbf{D}^2\, \hat{\mathbf{v}} \cdot \hat{\mathbf{v}}^* \mathrm{d}x\right) \ , \tag{32}$$

the production of fluctuating kinetic energy by shear of the basic flow K_f :

$$K_f = -\mathrm{Re}\left(\int_x w_0'\, \hat{u}\, \hat{w}^* \mathrm{d}x\right) \ , \tag{33}$$

the work done by buoyancy forces K_b :

$$K_b = \mathrm{Re}\left(\int_x Gr\, \hat{\theta} (\hat{\mathbf{e}}_z \cdot \hat{\mathbf{v}}^*) \mathrm{d}x\right) \ , \tag{34}$$

the dissipation of fluctuating kinetic energy by magnetic forces K_m :

$$K_m = -\mathrm{Re}\left(\int_x Ha^2 (\hat{w}\, \hat{w}^*) \mathrm{d}x\right) \ . \tag{35}$$

The rate of change of the fluctuation thermal energy Θ:

$$\mathrm{Re}\left(\frac{\mathrm{d}\Theta}{\mathrm{d}t}\right) = \mathrm{Re}\left(\lambda \int_x \hat{\theta}\, \hat{\theta}^* \mathrm{d}x\right) = \Theta_d + \Theta_1 + \Theta_2 \ , \tag{36}$$

where $\Theta = \int_x \hat{\theta}\, \hat{\theta}^* \mathrm{d}x$, with the dissipation of fluctuating thermal energy Θ_d :

$$\Theta_d = \mathrm{Re}\left(\int_x \frac{1}{Pr} \mathbf{D}^2\, \hat{\theta} \cdot \hat{\theta}^* \mathrm{d}x\right) \ , \tag{37}$$

the production of fluctuating thermal energy by horizontal transport of temperature Θ_1:

$$\Theta_1 = -\mathrm{Re}\left(\int_x T_0'\, \hat{u}\, \hat{\theta}^* \mathrm{d}x\right) \ , \tag{38}$$

the production of fluctuating thermal energy by vertical transport of temperature Θ_2:

$$\Theta_2 = 0 \ . \tag{39}$$

The negative values of energy contributions characterise stabilizing dissipative terms, while the positive contributions are by nature destabilizing.

In the problems considered here the energy analysis results are given at the critical thresholds. According to the neutral stability condition, for $\lambda_r = 0$ the disturbances are neither amplified nor damped, thus $\frac{\mathrm{d}K}{\mathrm{d}t} = \frac{\mathrm{d}\Theta}{\mathrm{d}t} = 0$. Since the critical eigenvectors are defined to within a multiplicative constant, the energy equations specific terms also can be given to within a multiplicative constant. In order to present well-defined energy balances, the energy equations are scaled by the corresponding dissipation terms:

$$\bar{K}_d = \bar{K}_f + \bar{K}_b + \bar{K}_m = 1 \ , \tag{40}$$

$$\bar{\Theta}_d = \bar{\Theta}_1 + \bar{\Theta}_2 = 1 \ , \tag{41}$$

where the scaled terms are denoted with an overbar.

To compare the kinetic and thermal energy contributions, the following dimensionless ratio is given:

$$R = \frac{1}{Gr}\frac{K_d}{\Theta_d} \ , \tag{42}$$

For the fluctuating thermal energy, in general the dissipation term is balanced by vertical and horizontal temperature transport. In this case, as the basic temperature profile is independent of the $z-$ direction, the only contribution balancing dissipation $\bar{\Theta}_d$ is due to horizontal transport of temperature $\bar{\Theta}_1$:

$$\bar{\Theta}_d = \bar{\Theta}_1 = 1 \ . \tag{43}$$

V. LINEAR STABILITY RESULTS

The problem has been solved numerically by the Chebyshev spectral collocation method. The Matlab code created for the purpose of this project has been tested on simplified problems, for which the results have already been obtained by a number of authors. Additionally a comparison has been made with the results for $Ha = 0$ at the same conditions[10] and a good agreement provides a further check on the numerical accuracy.

The convergence of the numerical solution has been verified by varying the number of collocation points N, ensuring a reasonable accuracy of determination of the critical parameters. The number of collocation points required to meet a prescribed convergence criterion in the case of a liquid metal ($Pr = 0.015$) are presented in Table I. The critical Grashof numbers are accurate to $6th$ significant figure at relatively low cost for moderate values of the Hartmann number, up to $Ha = 200$. Further increase of Ha considerably increases the computational cost and the convergence criterion is lowered to 4 significant figures. At $Ha \sim 1000$ the convergence becomes slower and the number of significant figures decreases.

6 digit convergence	
Ha	N
10	23
50	36
100	49
200	67

4 digit convergence	
Ha	N
200	56
400	102
600	119
600*	159

TABLE I. Minimum number of collocation points N required for the convergence (6 digits for low and moderate Ha and 4 digits for high Ha) for $Pr = 0.015$. The * symbol denotes the secondary, more stable Mode 2.

It has already been shown by other authors[9,11], that in the absence of an externally applied magnetic field, as well as for low values of the Hartmann number, the marginal stability curve is continuously transformed when Pr increases. The obtained numerical results show a considerable distortion of the marginal stability curve with the increasing values of both Prandtl and Hartmann numbers.

The stability curves calculated for $Ha = 100$, are shown in Figure 4. For $Pr \leq 0.1$ the curve has a single minimum (Mode 1), corresponding to a hydrodynamic instability mode. For $Pr > 0.1$, the second minimum (Mode 2) is formed by continuous transformation of the neutral curve. The nature of Mode 1 also changes from dynamic to mixed with significant thermal component (see Table II below). The most unstable (most dangerous) mode corresponds to the absolute minimum of the stability curve.

Further increase of the value of Prantdl number results in a formation of a cusp and then a closed loop of the neutral curve. For higher values of Pr we observe the shift of the wavenumber values, as well as rather interesting shape of the curve. For $Ha = 0$ the loop is well-formed, while for finite Ha it becomes very narrow. The lower branch of the curve is pulled towards higher wavenumbers and forms a spear-shaped distortion (e.g. see $Pr = 3$ in Figure 5a).

The formation of a loop is associated with the interaction between neighbouring levels of the complex eigenvalue. The characteristic cross point D in Figure 5a corresponds to the intersection of two highest eigenvalues at the neural point $\lambda_r = 0$. For $Ha = 100$ and $Pr = 3$ it occurs at $k \simeq 2.3$. For $k > 2.3$ the intersection takes place at negative values of λ_r, while for $k < 2.3$, it occurs above the neutral stability level (Figure 5b), causing the formation of the loop. Within the loop it is the second highest eigenvalue (as an extension of the maximum growth rate) taking values of $\lambda_r = 0$ (Figure 5b) and marking the onset of instability.

A number of interesting features of the marginal stability curve can already be observed at moderate values of the Hartmann number (see $Ha = 10$ in Figure 6a). It happens, that the appearance and shape of the loop depends on the interaction between three highesteigenvalue levels, as shown in Figure 6b for $Ha = 10$ and $Pr = 10$. It also happens that, for certain values of parameters, a local minimum of the more stable Mode 2 occurs within the loop, as shown in the same example.

Another interesting distortion of the marginal curve occurs when the highest eigenvalue (maximum growth rate) crosses the neutral level of $\lambda_r = 0$ multiple times, yet the formation of a loop is impossible at this wavenumber as the interaction between the two levels takes place at negative values of λ_r, as shown for $Ha = 10$ and $Pr = 8$ in Figures 6a and 6b.

The variation of the eigenvalue spectra and resulting stability curves, depending both of the Prandtl and Hartmann numbers, is rather complex. For values of $Ha \sim 100$ and $Pr \sim 10$ and higher we observe a formation of yet another minimum (Mode 3), appearing at higher wavenumber values, within the elongated tongue-shaped distortion, as shown in Figure 7 (characteristic point M).

Moreover, in the range of Ha between 60 and 200 we have found a fourth local minimum on the branch of the curve that is totally disconnected from the main one. This minimum corresponds to the so-called Hartmann mode and is related to the instability of the Hartmann layers of thickness $O(Ha^{-1})$ at the duct walls (Mode 4). Extension of this mode to lower and higher values of Ha has proved to be very difficult owing to the limits of current computational resources. We discuss this mode in Conclusions.

The dependence of the critical Grashof number, critical wavenumber and critical frequency on Pr, for different values of the Hartmann number, are shown in Figures 8 and 9. The results show that for the lowest values of the Prandtl number, ($Pr < 10^{-2}$), where thermal effects are negligible due to very effective heat conduction, the critical Grashof number reaches an asymptotic relation of $Gr_{cr} \simeq aPr^{-1}$, so that the critical Rayleigh number, $Ra_{cr} = Pr\, Gr_{cr} = a$. Here the coefficient a depends on the Hartmann number and increases for the higher values of the applied magnetic field. In general, the increase of Ha has stabilizing effects on the flow, while the increase of Pr destabilises it.

As Ra becomes the governing parameter, the instability clearly has hydrodynamic origin and is modified by variation of the basic velocity profile only without any effects of thermal perturbations.

For $Ha \to 0$ the effect of thermal perturbations, namely the sudden decrease of the critical wavenumber and a frequency jump, is observed at $Pr \sim 10^{-1}$, as discussed in Refs. 9 and 11. A departure from the purely hydrodynamical formulation is shown in Figure 8, where an additional curve represents the solution of the Orr-Sommerfeld boundary

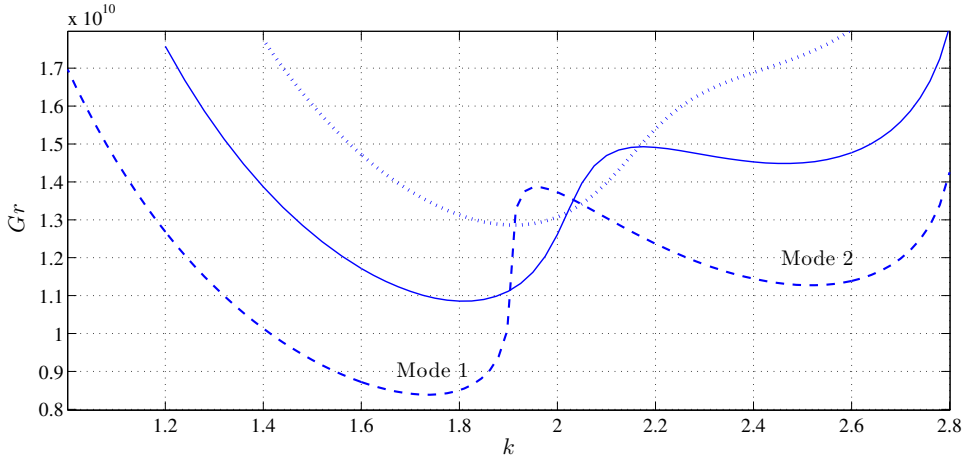

FIG. 4. Marginal stability curves for $Ha = 100$ and $Pr = 0.1$ (dotted line), $Pr = 0.12$ (solid line), $Pr = 0.15$ (broken line).

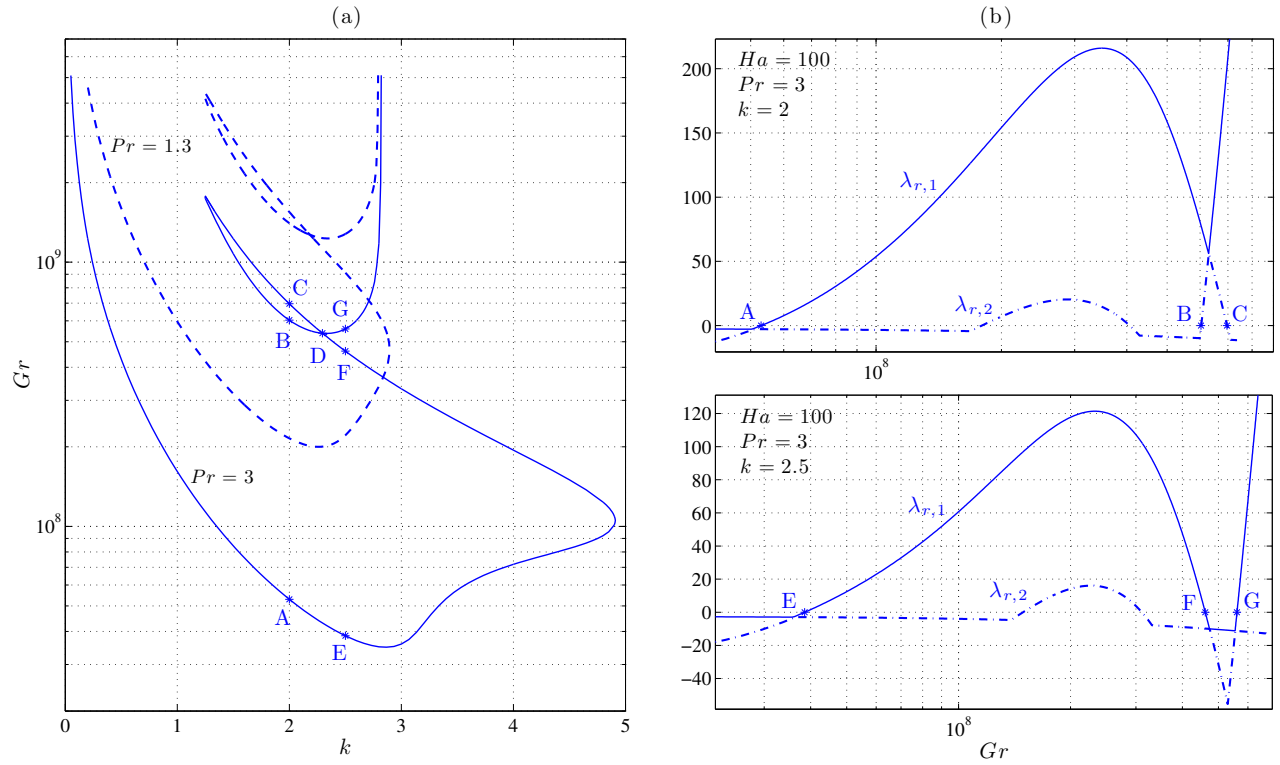

FIG. 5. Neutral stability curves for $Ha = 100$ at $Pr = 1.3$ (broken line) and $Pr = 3$ (solid line) (a) and the corresponding highest eigenvalue levels (b) for $k = 2$ (top) and $k = 2.5$ (bottom). The maximum growth rate $\lambda_{r,1}$ and the second highest eigenvalue $\lambda_{r,2}$ mark the onset of instability at points $A - E$.

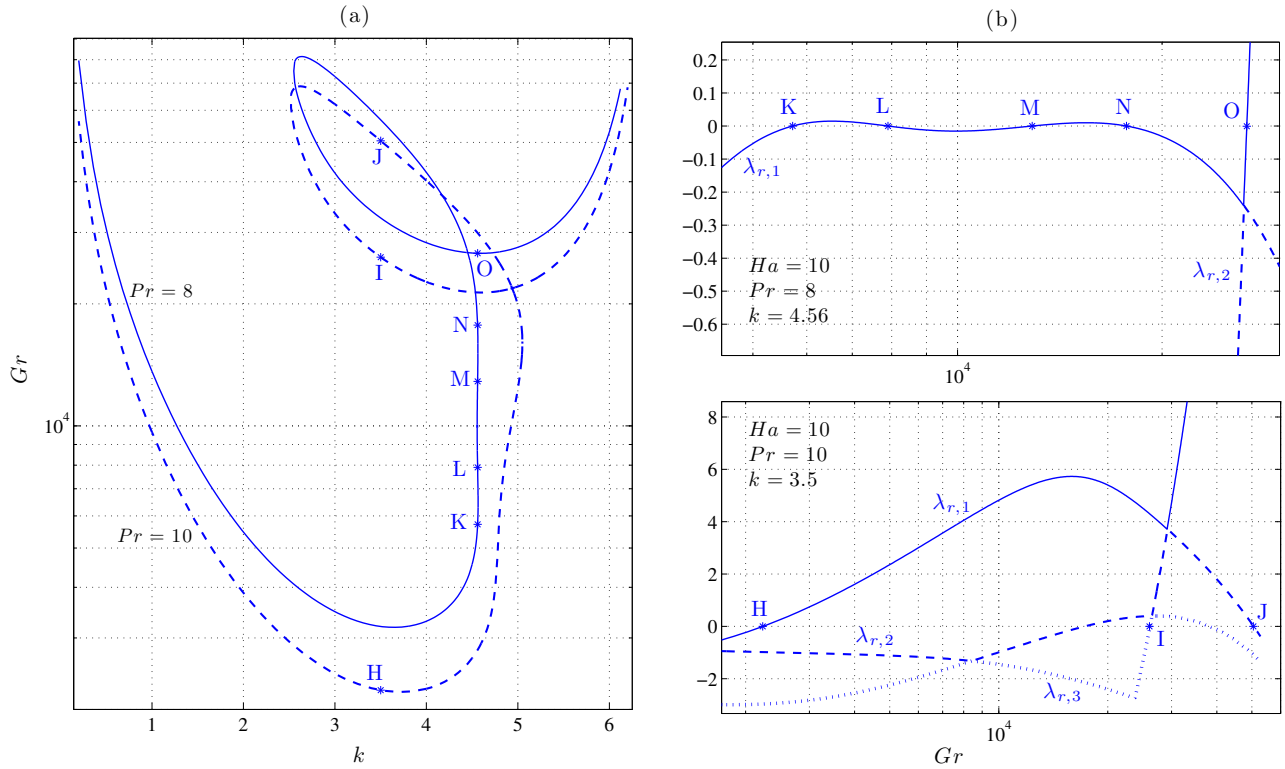

FIG. 6. Neutral stability curves for $Ha = 10$ at $Pr = 8$ (solid line) and $Pr = 10$ (broken line) (a) and the corresponding highest eigenvalue levels (b) for $k = 4.56$ (top) and $k = 3.5$ (bottom). The maximum growth rate $\lambda_{r,1}$, the second highest $\lambda_{r,2}$ and the third highest eigenvalue $\lambda_{r,3}$ mark the onset of instability at points $H - O$.

value problem with a given velocity profile[8]. For $Pr \to 0$ and in the absence of an external magnetic field, both the critical wavenumber and critical frequency tend to unique limits of $k_{cr} = 4.15$ and $f_{cr} = 37.10$, respectively. Similar behaviour is observed for small and moderate values of Ha, as shown for $Ha = 10$ in Figure 8 (here the unique limits are $k_{cr} = 4.36$ and $f_{cr} = 85.56$).

For higher values of Ha, thermal effects are observed at much lower values of the Prandtl number. In contrast to the non-magnetic case, the critical wavenumber and frequency values do not tend to unique limits, even for Pr as low as 10^{-4}. The jump in the wavenumber (associated with the formation of a loop within the marginal stability curve) gradually shifts towards lower values of Pr and is followed by a sudden wavenumber increase for higher Pr, which corresponds to the stretching of marginal stability curves (see $Ha = 100$ and $Ha = 200$ in Figure 9). The contour plots illustrating temperature disturbance isotherms and disturbed velocity streamlines are presented for $Ha = 100$ in Figure 11.

At high values of the Prandtl number, $Pr \gg 1$, where thermal effects are most pronounced, the critical values of frequency and the Grashof number asymptotically decrease for all values of Ha.

The instability mode corresponding to the loop formation (Mode 2) for the case of $Ha \to 0$ follows closely the Orr-Sommerfeld solution[8]. The increase of the Hartmann number shifts the appearance of this mode towards lower Prandtl numbers. For the range of Ha considered here, the critical Grashof number decreases as $Gr_{cr} \sim Pr^{-1}$, while both the critical wavenumber and critical frequency values tend to constant limits (see Figures 8 and 9). The increasing magnetic field strongly affects this instability, as shown in Figure 12, where the contour plots of temperature disturbance isotherms and disturbed velocity streamlines are presented for the sample value of $Pr = 7.01$. It is noticeable that the temperature disturbance moves towards the walls as Ha increases, together with the inflection points.

The appearance of the third kind of instability, corresponding to the stretching of neutral stability curves (Mode 3), is first observed at $Pr \sim 10$ for $Ha \sim 100$. This instability mode follows closely the most unstable mode at higher frequency and much higher wavenumber values, as shown in Figure 9 for $Ha = 100$ and 200. Contour plots of disturbed temperature isotherms and velocity streamlines (Figure 13) show clearly, that these instabilities are located near the vertical boundaries.

The dependence of the critical Grashof number, critical wavenumber and the corresponding frequency on the Hartmann number, for the sample values of the Prandtl number corresponding to liquid metals ($Pr = 0.015$) and to Flibe ($Pr = 38.055$) is shown in Figure 10. For $Ha \to 0$ the critical values of parameters, for all the instabilities discussed above, tend to unique limits. The externally applied magnetic field, stabilizing the flow, shifts the onset of instabilities to higher values of Gr, which is accompanied for all of the instability modes by the increase in frequency.

For the most unstable Mode 1, corresponding to the hydrodynamic minimum of the marginal stability curve, the critical wavenumber increases for $Ha \gtrsim 1$, until it reaches its maximum value (at $Ha \simeq 9$ for $Pr = 0.015$ and $Ha \simeq 120$ for $Pr = 38.055$ in Figure 10). The increase is more pronounced for higher values of Pr. Further increase of the Hartmann number shifts the critical wavenumber towards lower values, increasing the size of the marginal cells. The critical values of the Grashof number and frequency for this most unstable mode reach asymptotic relations at the highest values of the Hartmann number ($Ha > 200$).

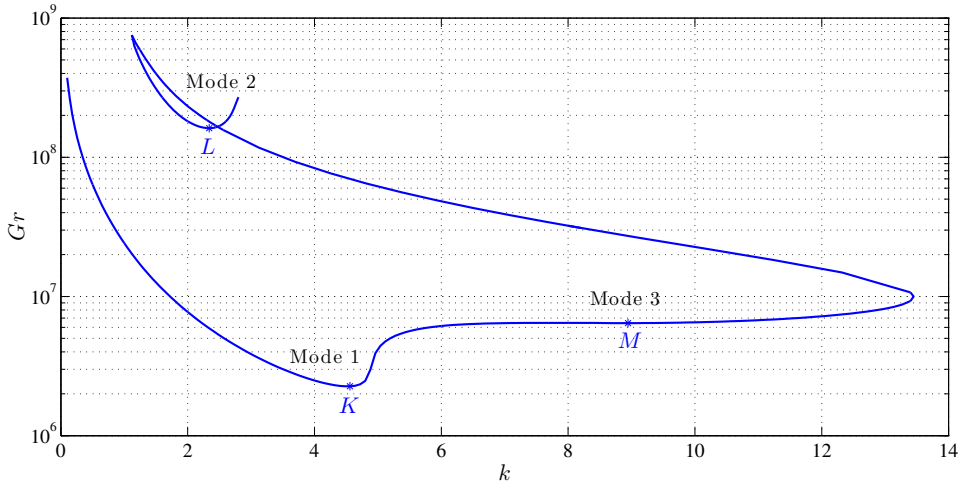

FIG. 7. Neutral stability curve for $Ha = 100$ and $Pr = 10$.

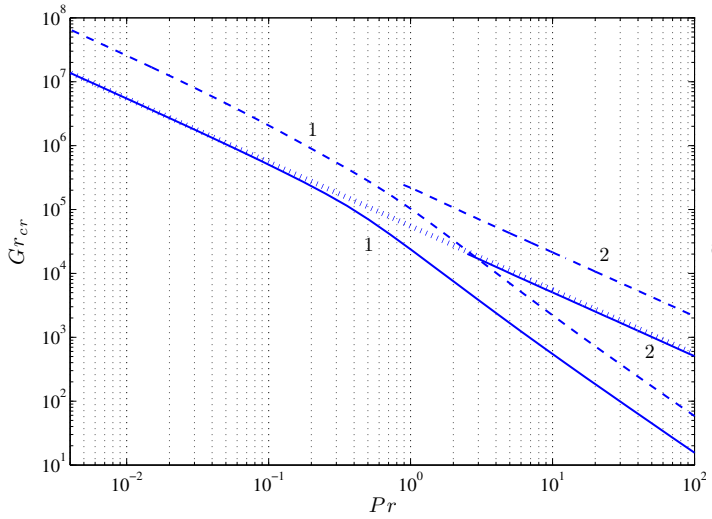

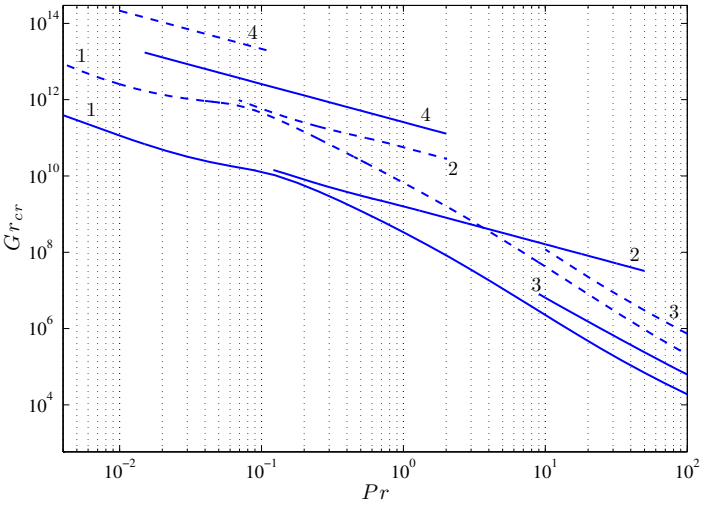

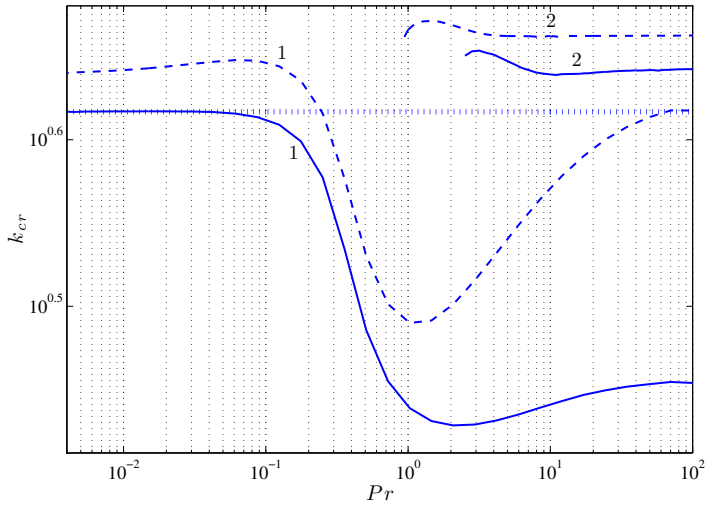

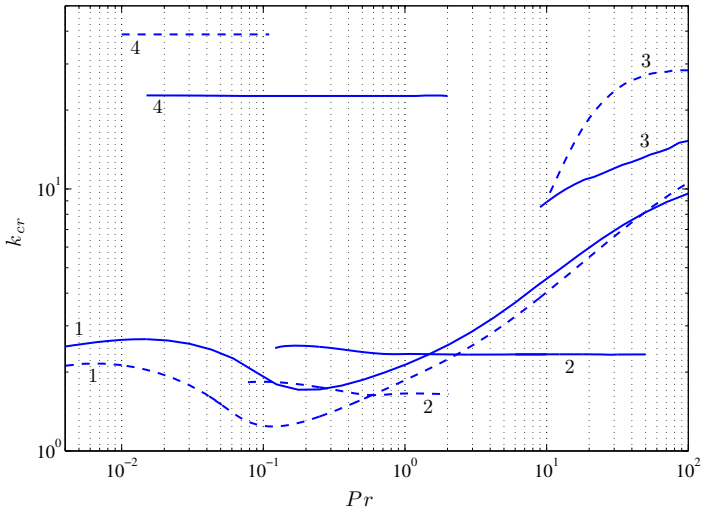

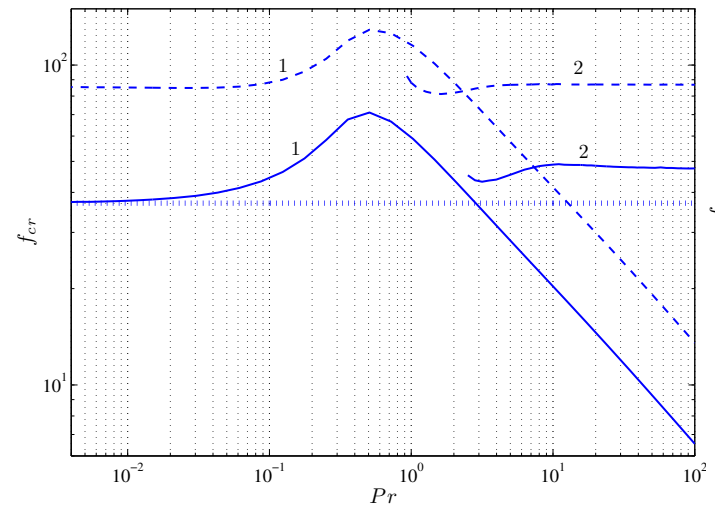

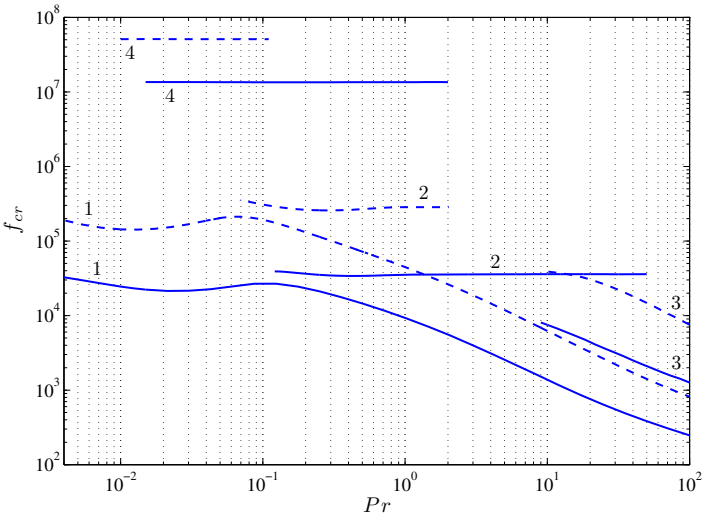

FIG. 8. Critical values of parameters for $Ha = 0$ (solid lines) and $Ha = 10$ (broken lines), Modes 1 and 2. Additional dotted line represents the Orr-Sommerfeld solution for $Pr = 0$.

FIG. 9. Critical values of parameters for $Ha = 100$ (solid lines) and $Ha = 200$ (broken lines), Modes 1-4.

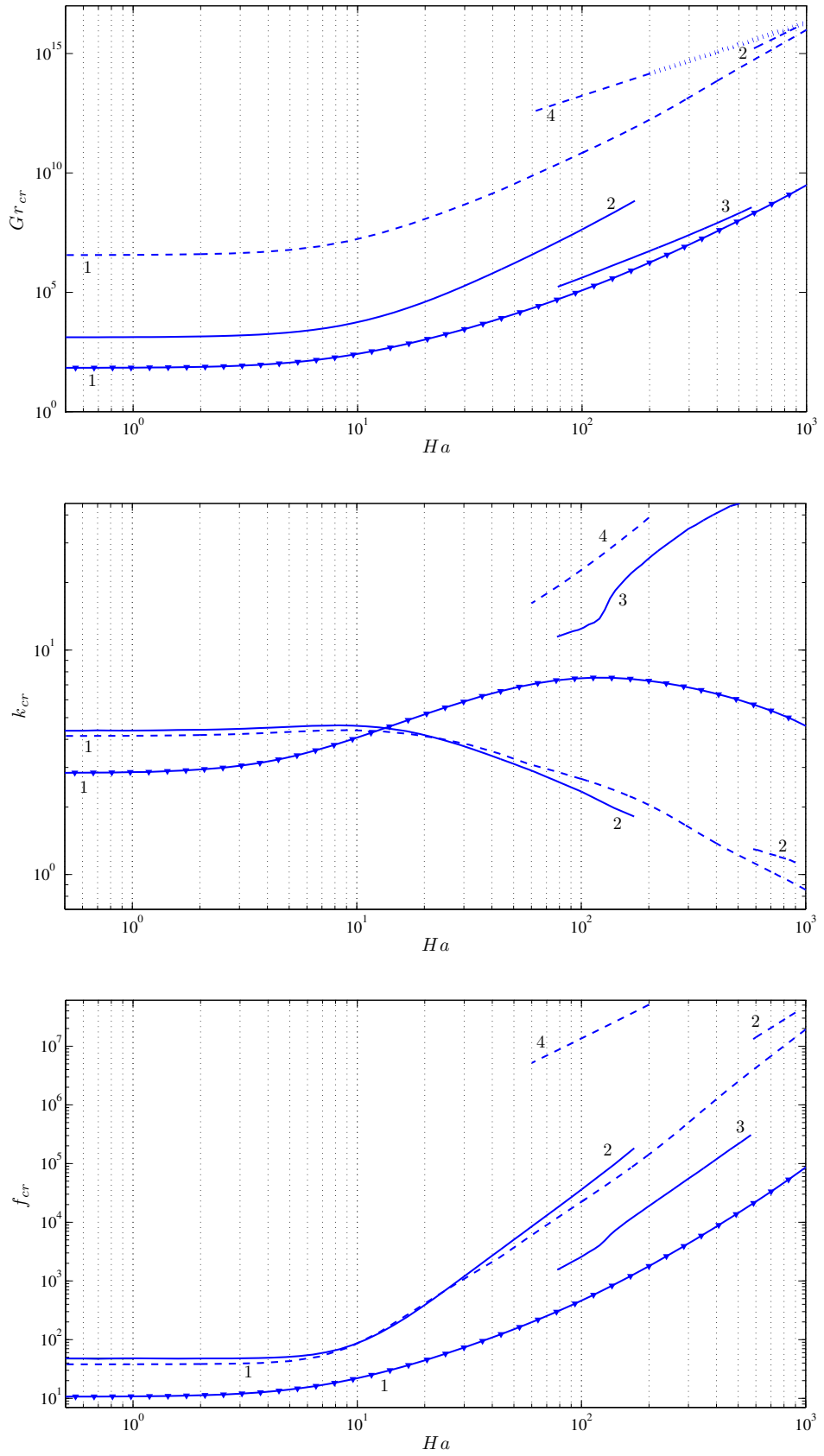

FIG. 10. Critical values of parameters for $Pr = 0.015$ (broken lines, Modes 1,2,4) and $Pr = 38.055$ (solid lines, Modes 1,2,3). Additional markers $\triangledown$ indicate the most unstable mode, additional dotted line represents the asymptotic extension of Mode 4

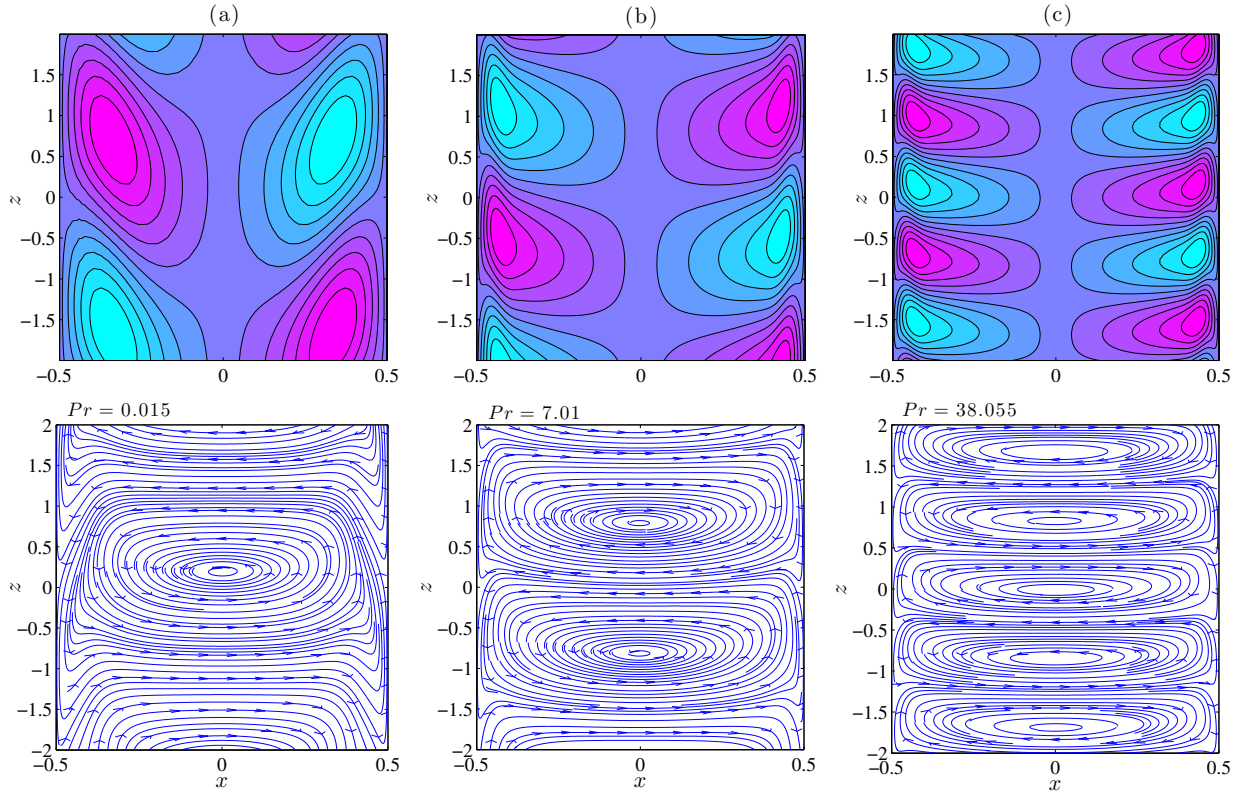

FIG. 11. Contours plots of the most unstable Mode 1 for $Ha = 100$. Temperature disturbance isotherms (top) and disturbed velocity streamlines (bottom) calculated at $Pr = 0.015$ (a), $Pr = 7.01$ (b) and $Pr = 38.055$ (c).

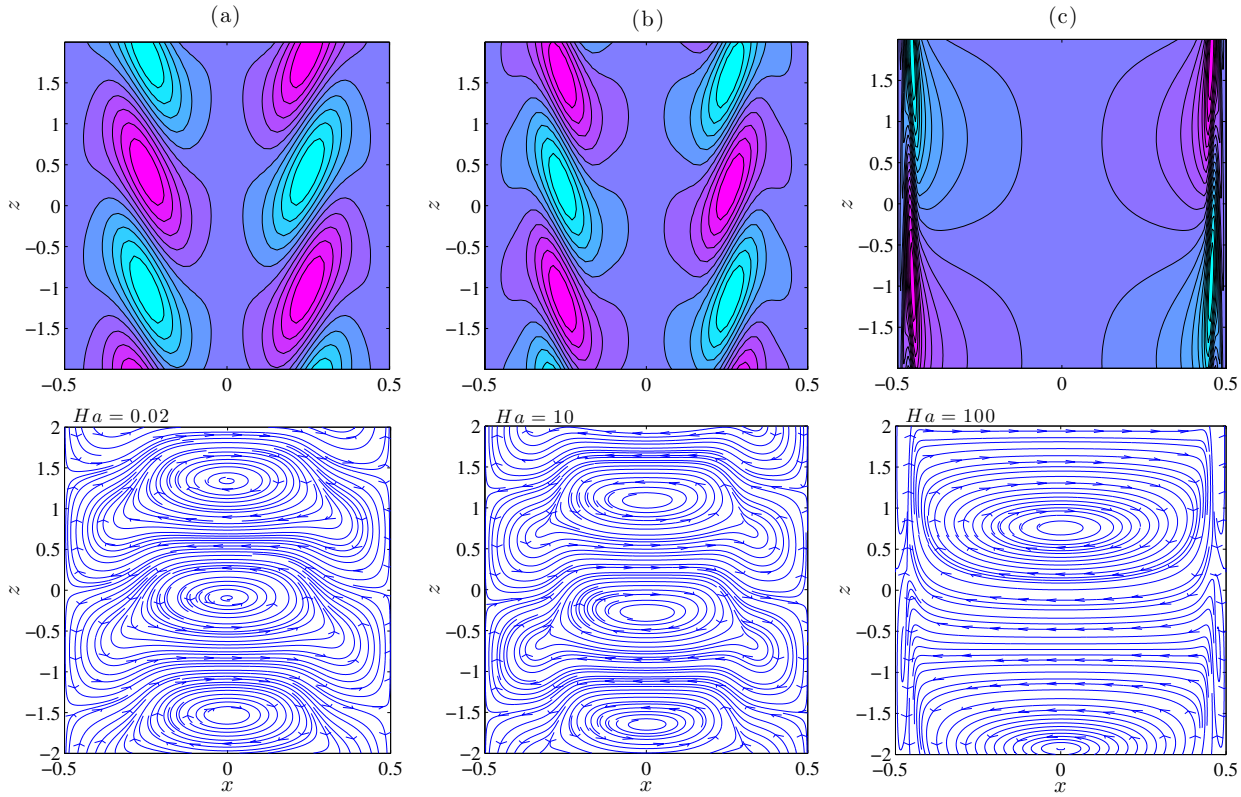

FIG. 12. Contours plots of Mode 2 for $Pr = 7.01$. Temperature disturbance isotherms (top) and disturbed velocity streamlines (bottom) calculated at $Ha = 0.02$ (a), $Ha = 10$ (b) and $Ha = 100$ (c).

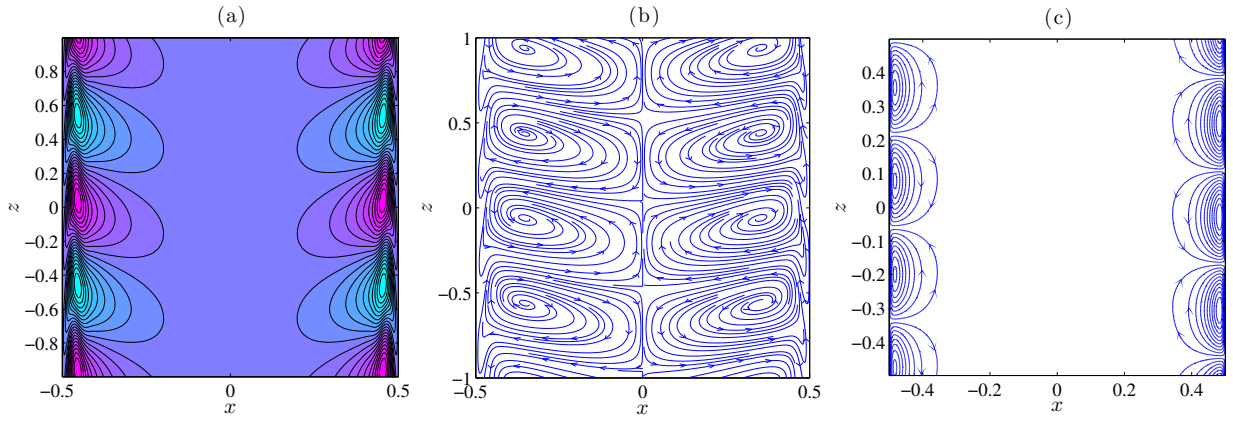

FIG. 13. Contour plots of Mode 3 and 4 for $Ha = 100$. Temperature disturbance isotherms (a) and disturbed velocity streamlines (b) calculated for Mode 3 at $Pr = 38.055$. Disturbed velocity streamlines of Mode 4 (c) calculated at $Pr = 0.015$.

The more stable Mode 2, corresponding to the formation of the loop in the marginal stability curve, appears for $Pr = 38.055$ at the whole range of Ha considered here and is very efficiently stabilised by the magnetic field. The quick increase of Gr_{cr} is accompanied by the decrease of the critical wavenumber. For liquid metals, this instability mode appears at very high values of Ha ($Ha \simeq 580$ for $Pr = 0.015$ as shown in Figure 10), with higher critical wavenumber and frequency values than the corresponding most unstable mode.

The instability mode appearing due to the stretching of marginal stability curve (Mode 3) is observed for $Pr = 38.055$ at $Ha \geq 78$. The magnetic field stabilises this mode less efficiently, as shown in Figure 10. The critical wavenumber increases very quickly with the increasing Ha, which corresponds to a strong decrease of the size of the marginal cells.

A summary of the fluctuating energy budget for each of the instability modes discussed is given in Tables II−IV. For the most unstable Mode 1 at the lowest values of Pr the ratio of dimensionless kinetic and thermal dissipation ($R \gg 1$) indicates indeed a purely dynamical origin. For the lowest values of the Hartmann number (see $Ha = 0.02$ in Table II, the negligible effects of buoyancy at $Pr \ll 1$ gain importance and take over as the main destabilizing contribution in the kinetic fluctuating energy balance for $Pr \sim 1$. At higher values of the Prandtl number this instability mode changes its nature due to the increasing importance of thermal dissipation ($R < 1$). At $Pr = 38.055$, corresponding to Flibe, the most unstable mode manifests as a thermal wave.

For low and moderate values of the applied magnetic field (see $Ha = 10$ in Table III), a similar behaviour to the non-magnetic case can be observed at the lowest values of Pr, with the additional stabilizing effects of the magnetic field. With the increase of Pr, the fluctuating energy contribution due to buoyancy very quickly takes over as the main destabilizing factor, while the energetic contribution due to shear of mean flow remains negligible for $Pr \gtrsim 1$. The stabilizing contribution of the magnetic field remains then at the order of kinetic energy dissipation.

Pr	$\bar{K_f}$	$\bar{K_b}$	$\bar{K_m}$	R
Mode 1 (most unstable)				
10^{-2}	0.990	0.010	0	13382
0.015	0.985	0.015	0	5985
0.5	0.419	0.581	0	13.12
1	0.175	0.825	0	7.223
2.5	0.042	0.958	0	3.788
7.01	0.004	0.996	0	2.014
10	0.001	0.999	0	1.638
38.055	0	1	0	0.778
Mode 2				
2.5	0.390	0.610	0	2.551
7.01	0.304	0.696	0	1.176
10	0.283	0.717	0	0.879
38.055	-0.385	1.385	0	0.099

TABLE II. Energy balance for $Ha = 0.02$

Pr	$\bar{K_f}$	$\bar{K_b}$	$\bar{K_m}$	R
Mode 1 (most unstable)				
10^{-2}	1.603	0.042	-0.645	2545
0.015	1.583	0.062	-0.645	1152
0.1	1.303	0.379	-0.682	35.26
0.5	0.355	1.846	-1.201	5.012
1	0.023	2.394	-1.417	3.161
2.5	-0.084	2.470	-1.387	1.681
7.01	-0.062	2.278	-1.216	0.851
38.055	-0.017	2.019	-1.002	0.314
Mode 2				
1	0.465	1.096	-0.561	3.104
5	0.239	1.224	-0.463	1.146
7.01	0.215	1.231	-0.446	0.899
38.055	-0.462	1.735	-0.273	0.099

TABLE III. Energy balance for $Ha = 10$

Pr	$\bar{K_f}$	$\bar{K_b}$	$\bar{K_m}$	R
Mode 1 (most unstable)				
10^{-2}	-0.05	13.42	-12.37	61.33
0.015	-1.41	16.86	-14.45	38.15
0.1	-7.64	36.96	-28.32	14.88
1	-8.00	56.49	-47.49	2.573
2.5	-5.28	59.97	-53.69	0.999
7.01	-2.10	54.50	-51.40	0.318
38.055	-0.17	20.02	-18.85	0.087
Mode 2				
0.15	-2.367	11.092	-7.725	18.43
1	-2.253	9.644	-6.391	9.537
7.01	-2.188	6.994	-3.806	3.358
38.055				
Mode 3				
10	-1.010	8.840	-6.830	0.285
20	-0.611	8.243	-6.632	0.143
38.055	-0.341	7.594	-6.253	0.083
Mode 4				
0.015	1.024	-0.001	-0.023	10^6
0.1	1.025	-0.002	-0.023	10^6
2	1.025	-0.002	-0.023	10^4

TABLE IV. Energy balance for $Ha = 100$

At $Ha = 10$ thermal dissipation dominates over the kinetic one already at the values of Pr corresponding to water-based electrolytes, changing the nature of this instability. For high values of the Hartmann number (see $Ha = 100$ in Table IV), buoyancy serves as the main destabilizing factor already at the values of Prandtl numbers corresponding to liquid metals and is balanced by a strong magnetic field. The fluctuating kinetic energy contribution due to shear of mean flow serves here as an additional stabilizing term, negligible at low and high values of Pr.

For the less dangerous Mode 2, corresponding to the formation of a loop, the ratio of kinetic to thermal dissipation at its appearance ($R > 1$) confirms the dynamic origin of this mode. Here the kinetic fluctuating energy contribution due to buoyancy serves as the main destabilizing factor for all values of Ha considered (Tables II-IV).

At the lowest values of Ha (see $Ha = 0.02$ in Table II, the energetic contribution due to shear of mean flow serves as a secondary destabilizing factor, while for the higher values of Pr, at the range corresponding to Flibe, becomes a negative stabilizing contribution. This corresponds to the sudden increase of thermal effects, with the thermal dissipation dominating over the kinetic one ($R < 1$) for $Pr \gtrsim 10$.

Very similar energy balance is observed at low and moderate values of the Hartmann number (see $Ha = 10$ in

Table III), with the additional stabilizing effects of low magnetic field and the thermal dissipation gaining importance at slightly lower values of Pr, changing the nature of this instability at the values corresponding to water based electrolytes. With the increase of the Hartmann number (see $Ha = 100$ in Table IV), more similarities between this secondary instability (Mode 2) and the most unstable one (Mode 1) are observed. The energetic contribution due to buoyancy serves as the main destabilizing term and is balanced by a strong stabilizing magnetic factors and a stabilizing contribution due to shear of the basic flow.

The third mode of instability, corresponding to stretching of the marginal stability curve and appearing at higher values of Ha and Pr (see $Ha = 100$ in Table IV) is of thermal origin, as indicated by the dissipation ratio $R < 1$. The thermal dissipation dominates at the appearance of this mode and becomes stronger with the increase of Pr. In the kinetic energy balance, the contribution due to buoyancy is again the only stabilizing factor, balanced by the strong magnetic term and a weaker contribution corresponding to shear of the basic flow.

VI. CONCLUSIONS

Stability of buoyant MHD convective flow in a vertical channel owing to internal heat sources has been studied. The Prandtl and Hartmann numbers have been varied in the wide range, which are relevant to fusion reactor blankets and laboratory experiments. The results show that up to four different local minima may exist on the marginal stability curve. For moderate magnetic field the leading instability has a mixed thermal-hydrodynamic origin and is shifted towards the walls as both the Hartmann and Prandtl number increase. It is interesting that this mode is highly damped by the magnetic field, which is somewhat surprising as the thermal effects are usually less damped than the hydrodynamic ones (see e.g. Ref. 22). As the Hartmann number increases, the critical Grashof number increases rapidly, so that the flow becomes very stable. However, the Hartmann mode, has also been discovered and calculations for this mode have been performed with good accuracy up to $Ha = 200$. This, however, is sufficient as the high$-Ha$ asymptotics has been reached as clearly seen in Figure 13. It turns out that for $Ha \sim 1000$ this mode, shown in Figure 12c, becomes most unstable.

Concerning various fluids − liquid metals and electrolytes − the critical Grashof number varies between them by orders of magnitude. Moreover, for flow visualization in the laboratory experiments on convection one should replace the liquid metals with electrolytes with great caution as the instabilities in them may be of completely different origin.

Naturally, the next steps in the understanding of the effect of internal heat sources on the flow stability should involve rectangular ducts with various thermal and electrical boundary conditions. For each of these combinations the basic temperature and velocity profiles will be different and so will be the nature of the instabilities.

Finally, two points should be added. First of all, we do not exclude the possibility of the appearance of the elevator modes, which have been discovered in many situations involving multiple vertical streams, see a brief review in Ref. 7. Secondly, extending the results to finite cavities with top and bottom lids should be done with caution as absolute instability may set in[24], which may lead to decay of convective instabilities and further breakup of wave-trains. These issues require a separate investigation.

REFERENCES

[1] M. Abdou, N. B. Morley, S. Smolentsev, A. Ying, S. Malang, A. Rowcliffe, and M. Ulrickson, "Blanket/first wall challenges and required R&D on the pathway to DEMO," Fusion Engineering and Design **100**, 2 – 43 (2015).

[2] L. Buhler, C. Mistrangelo, J. Konys, R. Bhattacharyay, Q. Huang, D. Obukhov, S. Smolentsev, and M. Utili, "Facilities, testing program and modeling needs for studying liquid metal magnetohydrodynamic flows in fusion blankets," Fusion Engineering and Design **100**, 55 – 64 (2015).

[3] L. Morgan and J. Pasley, "Tritium breeding control within liquid metal blankets," Fusion Engineering and Design **88**, 107 – 112 (2013).

[4] L. Barleon, U. Burr, K. Mack, and R. Stieglitz, "Heat transfer in liquid metal cooled fusion blankets," Fusion Engineering and Design **51 - 52**, 723 – 733 (2000).

[5] N. Vetcha, S. Smolentsev, and M. Abdou, "Stability analysis for buoynacy-opposed flows in poloidal ducts of the DCLL blanket," Fusion Science and Technology **60**, 518–522 (2011).

[6] N. Vetcha, S. Smolentsev, M. Abdou, and R. Moreau, "Study of instabilities and quasi-two-dimensional turbulence in volumetrically heated magnetohydrodynamic flows in a vertical rectangular duct," Physics of Fluids **25**, 024102 (2013).

[7] L. Liu and O. Zikanov, "Elevator mode convection in flows with strong magnetic fields," Physics of Fluids **27**, 044103 (2015).

[8] G. Gershuni, E. Zhukhovitskii, and A. Iakimov, "On the stability of steady convective motion generated by internal heat sources," Journal of Applied Mathematics and Mechanics **34**, 669 – 674 (1970).

[9] G. Gershuni, E. Zhukhovitskii, and A. Iakimov, "Two kinds of instability of stationary convective motion induced by internal heat sources," Journal of Applied Mathematics and Mechanics **37**, 544 – 548 (1973).

[10] M. Takashima, "The stability of natural convection in a vertical fluid layer with internal heat generation," Journal of the Physical Society of Japan **52**, 2364–2370 (1983).

[11]A. A. Kolyshkin, "On the stability of steady convective motion generated by internal heat sources in a magnetic field," Canadian Journal of Physics **66**, 990–993 (1988).
[12]U. Müller and L. Bühler, *Magnetofluiddynamics in Channels and Containers* (Springer, 2001).
[13]M. Lappa, *Thermal Convection: Patterns, Evolution and Stability* (Wiley, 2009).
[14]C. P. C. Wong, S. Malang, M. Sawan, I. Sviatoslavsky, E. Mogahed, S. Smolentsev, S. Majumdar, B. Merrill, R. Mattas, M. Friend, J. Bolin, and S. Sharafat, "APEX advanced ferritic steel, Flibe self-cooled first wall and blanket design," Journal of Nuclear Materials **329**, 1599–1604 (2004).
[15]O. Andreev, A. Thess, and C. Haberstroh, "Visualization of magnetoconvection," Physics of Fluids **15**, 3886–3889 (2003).
[16]E. M. de les Valls, L. Sedano, L. Batet, I. Ricapito, A. Aiello, O. Gastaldi, and F. Gabriel, "Lead-lithium eutectic material database for nuclear fusion technology," Journal of Nuclear Materials **376**, 353 – 357 (2008).
[17]A. Tiwari, B. Allison, J. Hohorst, R. Wagner, and C. Allison, "Insertion of lead lithium eutectic mixture in RELAP/SCDAPSIM Mod 4.0 for fusion reactor systems," Fusion Engineering and Design **87**, 156 – 160 (2012).
[18]R. Serrano-Lopez, J. Fradera, and S. Cuesta-Lopez, "Molten salts database for energy applications," Chemical Engineering and Processing: Process Intensification **73**, 87 – 102 (2013).
[19]J. Mao, S. Aleksandrova, and S. Molokov, "Joule heating in magnetohydrodynamic flows in channels with thin conducting walls," International Journal of Heat and Mass Transfer **51**, 4392 – 4399 (2008).
[20]W. Criminale, T. Jackson, and R. Joslin, *Theory and Computation of Hydrodynamic Stability*, Cambridge Monographs on Mechanics (Cambridge University Press, 2003).
[21]S. Kaddeche, D. Henry, and H. Ben Hadid, "Magnetic stabilization of the buoyant convection between infinite horizontal walls with a horizontal temperature gradient," Journal of Fluid Mechanics **480**, 185–216 (2003).
[22]A. Hudoba, S. Molokov, S. Aleksandrova, and A. Pedcenko, "Linear stability of buoyant convection in a horizontal layer of an electrically conducting fluid in moderate and high vertical magnetic field," Physics of Fluids **28**, 094104 (2016).
[23]J. C. R. Hunt, "On the stability of parallel flows with parallel magnetic fields," Proceedings of the Royal Society of London A: Mathematical, Physical and Engineering Sciences **293**, 342–358 (1966).
[24]S. M. Tobias, M. R. E. Proctor, and E. Knobloch, "Convective and absolute instabilities of fluid flows in finite geometry," Physica D Nonlinear Phenomena **113**, 43–72 (1998).